processes

MDPI

Article

Numerical Simulations for the Mechanical Behavior of a Type-B Sleeve under Pipeline Suspension

Haiping Tang [1,*], Yaping Ding [2], Guangyou Qiu [3], Ziguang Liu [1] and Zhibin Deng [1]

[1] College of Civil Aviation Safety Engineering, Civil Aviation Flight University of China, Deyang 618307, China; 18790896558@163.com (Z.L.); dengzb84@163.com (Z.D.)
[2] Department of Transportation and Municipal Engineering, Sichuan College of Architectural Technology, Chengdu 610399, China; dingsccat@126.com
[3] Dehong Oil and Gas Transportation Branch of Southwest Oil and Gas Pipeline Co., Ltd. of Pipe China, No. 6 Jinkongque Street, Mangshi 678400, China; qiugyou@163.com
* Correspondence: tang14187@cafuc.edu.cn

Abstract: The type-B sleeve is widely used for reinforcing defective pipelines. Due to the impact of suspension on pipeline safety, the behavior of the type-B sleeve structure has garnered increasing attention. In this study, we establish a numerical model of a defective pipeline reinforced with a type-B sleeve while accounting for the effects of the internal natural gas pressure and gravitational load. We investigate the influence of the sleeve length, suspended pipeline length, internal pressure, and sleeve position on the mechanical behavior of the type-B sleeve. The maximum values for Mises stress and axial strain were both observed near the edge of the suspended segment of the pipeline. For the type-B sleeve structure, the high Mises stress zone was at the bottom of the fillet weld; the axial strain near the fillet weld alternated between tension and compression along the axial direction. With an increase in internal pressure and suspended pipeline length, the Mises stress and axial strain of the type-B sleeve became more prominent. For sleeve length in the ranges of 1 to 3 m, the changes in the stress and strain did not exceed 10 MPa and 0.5×10^{-3}, respectively. However, the Mises stress and axial strain on the type-B sleeve structure were independent of the position of the defect on the pipeline. This study provides an important reference for type-B sleeve protection during suspension and other similar practical engineering applications.

Keywords: type-B sleeve; suspended pipeline; mechanical behavior; numerical simulation

check for updates

Citation: Tang, H.; Ding, Y.; Qiu, G.; Liu, Z.; Deng, Z. Numerical Simulations for the Mechanical Behavior of a Type-B Sleeve under Pipeline Suspension. *Processes* **2024**, *12*, 1585. https://doi.org/10.3390/pr12081585

Academic Editor: Jiaqiang E

Received: 19 May 2024
Revised: 23 July 2024
Accepted: 26 July 2024
Published: 29 July 2024

Copyright: © 2024 by the authors. Licensee MDPI, Basel, Switzerland. This article is an open access article distributed under the terms and conditions of the Creative Commons Attribution (CC BY) license (https://creativecommons.org/licenses/by/4.0/).

1. Introduction

Long-distance natural gas pipelines play an important role in energy transportation. However, defects such as corrosion and cracks often lead to a decrease in the strength of the pipeline, causing accidents and severe economic losses [1–3]. Timely reinforcement at defective locations is the main way to prevent such accidents. In general, the type-A sleeve, type-B sleeve, and composite sleeve are widely used in enhancing the strength of the defective pipeline [4–6]. However, the type-B steel sleeve, which attaches to the pipe by fillet welds, has significant advantages due to the axial sealing and high strength and has been widely employed in engineering practice [7,8].

As Figure 1 indicates, the local structure of a reinforced pipeline includes the sleeve, fillet welds, and the defective pipeline. Once the defective pipeline penetrates, the enclosed space formed by fillet weld and sleeve can prevent leakage. An experiment by Battelle laboratory [9] demonstrated that the blasting capacity of the pipeline repaired by the type-B sleeve reached or even exceeded the design pressure, which is highly useful for improving the bearing capacity. Yi et al. [10] investigated the burst pressure of a corroded X80 steel pipeline with a type-B repair sleeve and revealed that the local defective region exhibits the highest levels of stress, followed by the fillet weld. Unfortunately, buried pipelines are also subjected to additional geological loads, in addition to the internal pressure [11].

Wherever the foundation subsides, the bending moment increases at the cross-section of the buried pipeline. The stress caused by the settlement greatly affects the operational safety of pipelines. Therefore, the mechanical behavior of pipelines has always been a research concern [12,13]. The bending moment generated by a suspended pipeline can be particularly substantial, with the severe stress and strain concentrations on the structure of the type-B sleeve. Therefore, studying the mechanical behavior of pipelines suspended by geological subsidence is of great significance.

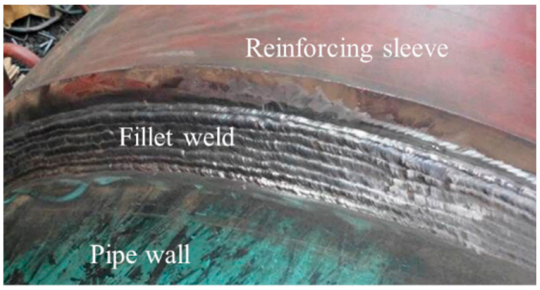


Figure 1. Type-B sleeve on a pipeline.

Previous studies have mainly focused on the mechanical behavior of pipelines with type-B sleeves under internal pressure. Due to rapid developments, the application of high-grade and large-diameter pipelines in gas transportation pipeline engineering continues to increase, such as the West–East Gas Transmission Project and the China–Russia Eastern Gas Pipeline. Compared to being only subjected to internal pressure, the mechanical behavior of type-B sleeves under pipeline suspension can be much more complex [14].

Therefore, in this study, we investigated the stress and strain experienced by type-B sleeves under buried gas pipeline suspension using Abaqus finite element analysis software. Particularly, the effects of pipeline suspension length, type-B sleeve position and length, internal pipeline pressure, and defect location on the mechanical behavior of type-B sleeves were studied. This study provides a theoretical foundation for designing and assessing pipelines reinforced with type-B sleeves.

2. Finite Element Model of Sleeve Repair Pipeline

2.1. Finite Element Model Parameters

To establish the finite element model, the structural dimensions were determined according to the "ASME B31.8—Gas Transmission and Distribution Piping Systems" specification. As shown in Figure 2, the relations between the dimensions of the type-B sleeve can be calculated as follows.

$$t_s = 1.4t \tag{1}$$

$$l_f = 1.4t + g_a \tag{2}$$

where t is the pipeline wall thickness; t_s is the sleeve wall thickness; g_a = 2.5 mm is the gap between the sleeve wall and pipeline wall; l_f is the length of the fillet weld leg; R is the internal diameter of the pipeline.

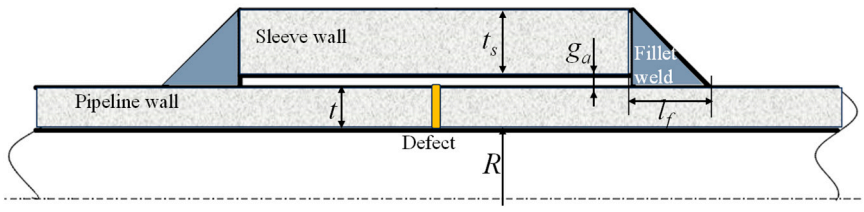


Figure 2. The diagrammatic sketch of type-B sleeve.

We selected the API 5L X80 pipeline with a diameter of 1422 mm and a wall thickness of 24 mm for simulation. Before suspension, the pipeline burial depth was set to 2.5 m

according to the "SY/T 6649-2018 Defect Repair of Oil & Gas Pipeline" Specification, and the sleeve wall thickness and the fillet weld leg length were calculated by Equations (1) and (2). The type-B sleeve is used to reinforce the strength of the defective pipeline wall. Therefore, the defect is considered in the finite element model, and its diameter is set to 20 mm. As Figure 3 demonstrates, the test pipeline can be divided into suspended and buried sections. To reduce the effect of the soil model on the mechanical behavior of the type-B sleeve, the soil model dimensions fixed its dimensions while appropriately increasing the height to 20 m × 6 m × 10 m [15].

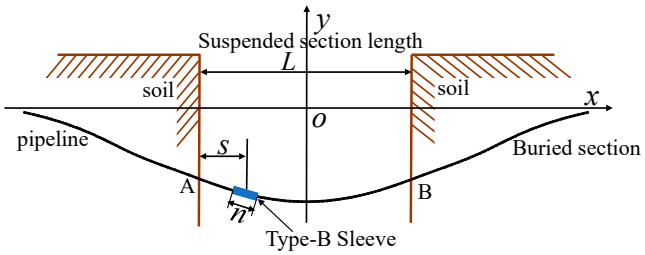


Figure 3. Diagram of the suspended pipeline.

2.2. Materials Properties

In general, the type-B sleeve uses the same material as the pipeline steel, and the weld of the sleeve is adopted based on equal strength matching with the pipeline steel. Therefore, the material properties of X80 steel are assigned to pipeline, sleeve, and fillet weld. For the API 5L X80 steel pipeline used in this study, the stress–strain curve of X80 pipeline steel is shown in Figure 4, and the Ramberg–Osgood model was used to describe the nonlinear model [16,17]. This is described by Equation (3), and the X80 pipeline streel properties are listed in Table 1.

$$\varepsilon = \frac{\sigma_t}{E}\left[1 + \alpha\left(\frac{\sigma_t}{\sigma_y}\right)^{n-1}\right] \tag{3}$$

where ε is the true strain of X80 steel; σ_t is tensile strength of X80 steel (MPa); σ_y is the yield strength of X80 steel (MPa); E is Young's modulus of X80 steel (GPa); n is the strain hardening exponent of X80 steel; α is the hardening coefficient of X80 steel.

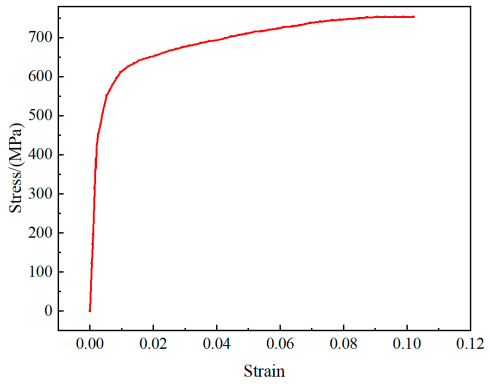


Figure 4. The stress–strain constitutive of the X80 pipeline steel.

Table 1. The property parameters of X80 pipeline steel.

Type	Density (kg/m^3)	Young's Modulus (MPa)	Poisson's Ratio	Yield Strength (MPa)	Tensile Strength (MPa)
X80 steel	8000	210	0.3	572	742

The mechanical behavior of the clay soil chosen in this study could be represented by the ideal elastic–plastic Mohr–Coulomb model [17]. The characteristic parameters of soil are listed in Table 2.

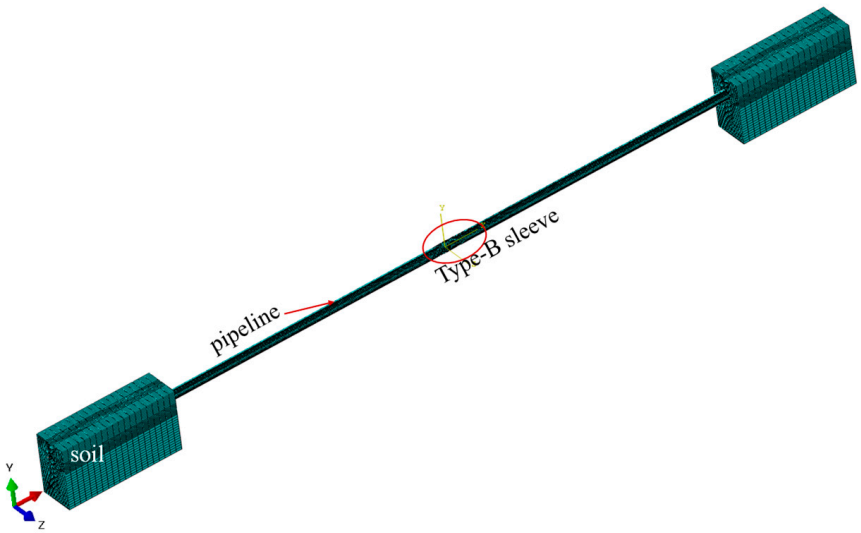
Table 2. Material properties of soil.

Type	Density (kg/m^3)	Elasticity Modulus (MPa)	Poisson's Ratio	Friction Angle (°)	Cohesion (kPa)	Dilatation Angle (°)
Clay	1950	50	0.3	22.5	30	0

2.3. Finite Element Model with Pipeline–Soil Interaction

To investigate the mechanical behavior of the suspended pipeline repaired by a type-B sleeve, the finite element model was established using the software Abaqus, which is shown in Figure 5a. The surface-to-surface interaction is used to describe the pipeline–soil contact relationship. In this model, we designated the pipeline's external surface and internal soil surface as the master surface and slave surface, respectively. Hard contact was applied to simulate the normal direction of the contact surface, while a penalty function method with a coefficient of 0.3 was employed to describe the tangential direction of the contact surface. Considering the quality of the grid and the geometric features of the finite element model, structured grid and hex elements were used to generate the mesh. Meanwhile, to ensure precision and computational efficiency, the element type was set as C3D8R. As shown in Figure 5b, due to the stress concentration at fillet weld and defects, the meshes were refined to improve the calculating precision.

During the suspension, the pipeline is supported by the soil. Therefore, the lateral and axial directions of the soil are less impacted by the loads of the suspended pipeline. To simulate actual working conditions, symmetric constrains were adopted at the plane of the soil and pipeline. The lower surface of the soil was fully fixed to maintain model stability, while its upper and suspended surfaces were free of constraints, which is shown in Figure 5c. Mechanical equilibrium is maintained between the pipeline soil before subsidence. Therefore, the natural gas pressure was employed, and a gravitational acceleration of $g = -9.8\ m/s^2$ along the Y-axis was applied to the model.



(**a**)

Figure 5. *Cont.*

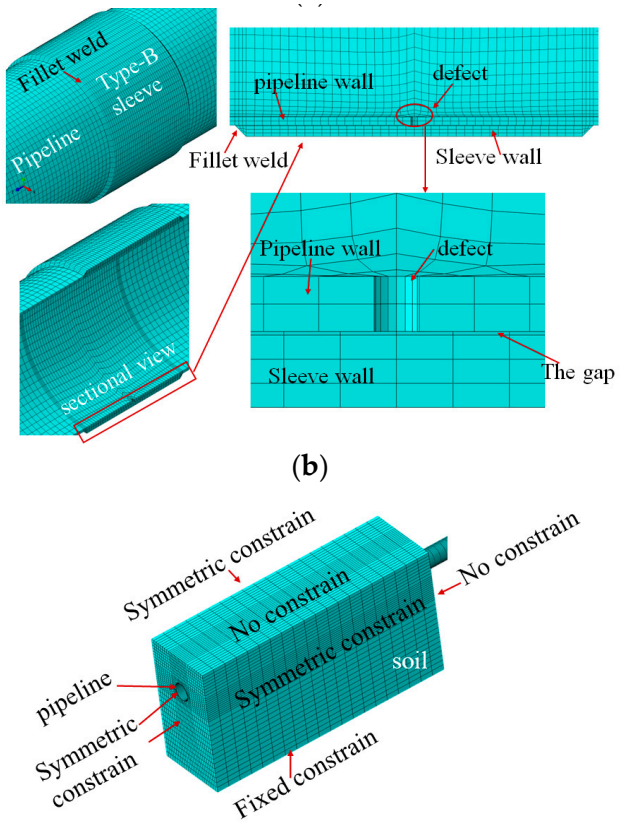


Figure 5. The numerical model of the suspended pipeline. (**a**) The finite model. (**b**) The enlarged view of the type-B sleeve model. (**c**) The boundary conditions.

2.4. Model Verification

When the length of the suspended pipeline is 300 m, the internal pressure is 12 MPa, and the length of the type-B sleeve is 1 m, the effect of the grid size of the type-B sleeve on the numerical results is calculated. As Table 3 lists, it can be found that the numerical simulation stabilized when the mesh size of the type-B sleeve is 33 mm, and the whole model consists of 333,152 elements.

Table 3. Mesh sensitivity results.

Gride Size (mm)	Gride Number	Maximum Displacement of Pipeline (m)	Maximum Mises Stress of Pipeline (Mpa)	Maximum Mises Stress of Type-B Sleeve (Mpa)
83	101,592	6.181	609	443
62.5	195,200	6.175	611	450
50	195,968	6.173	612	450
33	333,152	6.171	613	453
25	342,752	6.171	613	453
20	466,752	6.171	613	453

It is very difficult to verify the numerical model by experiment; thus, the numerical model was verified analytically. As shown in Figure 3, for the buried segment of the pipeline at each point, the gravity of the pipeline is equal to the support force of the soil, and the compression deformation of the soil is equal to the deflection of the pipeline. Equation (4) is presented according to Winkler elastic foundation beam theory [12].

$$EI\frac{d^4y}{d^4x} = q - ky \tag{4}$$

where q is the weight per unit length of pipeline; E is the elastic modulus of X80 pipeline steel; I is the cross-sectional moment of inertia of pipeline; y is the deflection of pipeline; k is the elastic resistance coefficient of soil.

The equilibrium equation on the pipeline cross-section can be given in Equations (5)–(7) [18].

$$\frac{dM(x)}{dx} = Q(x) \tag{5}$$

$$\frac{dQ(x)}{dx} = q \tag{6}$$

$$EIy'' = -M(x) \tag{7}$$

where $Q(x)$ is the shearing force, and $M(x)$ is the bending moment on the cross-section of the pipeline. The general solution can be expressed as Equation (8) [12]:

$$y = e^{\lambda x}(c_1 \cos \lambda x + c_2 \sin \lambda x) + e^{-\lambda x}(c_3 \cos \lambda x + c_4 \sin \lambda x) \tag{8}$$

where λ is the root of the characteristic equation; c_1, c_2, c_3, c_4 are the specific coefficients.

For the suspended segment of the pipeline, the differential equation of deflection can be represented as Equation (9) [19]:

$$EI\frac{d^2y}{d^2x} = M_B + S_B(y - y_B) + \frac{1}{2}qx^2 - \frac{1}{2}qLx \tag{9}$$

where M_B is the bending moment at point B in Figure 3, L is the length of the suspended pipeline, y_B is the displacement of point B in the Y-axis direction, and S_B is the equivalent axial tensile load calculated as:

$$S_B = \frac{\pi p d^2}{4} \tag{10}$$

where d is the outside diameter of the pipeline, and p is the internal pressure of the pipeline.

As Figure 6 indicates, both our numerical finite element model for pipeline suspended displacement and the theoretical results of Shang B. et al. [18] revealed the maximum settlement displacement to be at the middle of the pipeline. The analytical and numerical solutions for maximum settlement displacement were 5.8224 m and 6.1705 m, respectively. The error is 5.983% and lower than 6%. Therefore, the error meets the allowable range, and the accuracy of our model can be verified.

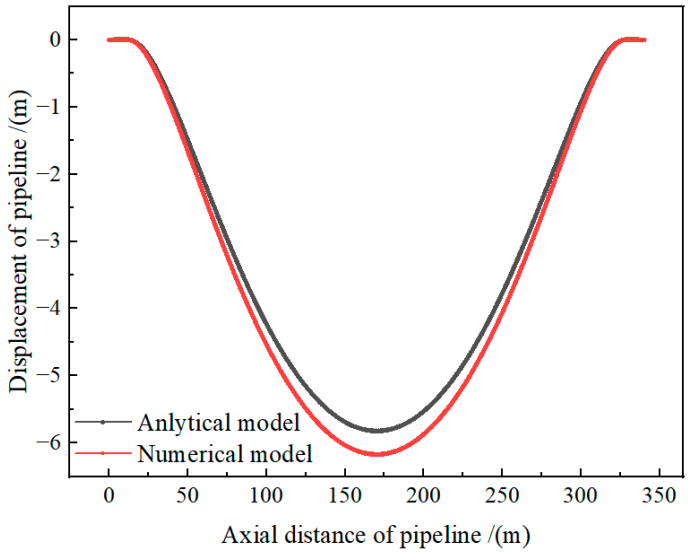


Figure 6. Comparison of the theoretical and numerical model.

3. Results and Discussion

3.1. The Influence of the Types of Defects

The types of defects on the pipeline are shown in Figure 7. If the defect on the type-B-sleeve reinforced pipeline penetrates the pipeline wall, natural gas will fill the space formed by the outer wall of the pipeline, the inner wall of the sleeve, and the fillet weld. Therefore, we conducted a comparative analysis of the mechanical behaviors of the reinforced pipeline under penetrating and non-penetrating defect conditions.

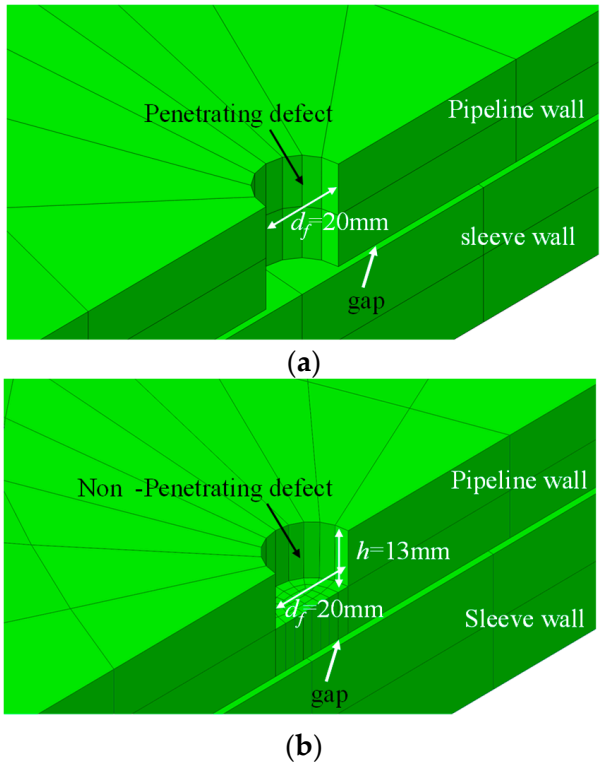


Figure 7. Diagrammatic representation of defect on the pipeline. (**a**) The penetrating defect. (**b**) The non-penetrating defect.

For the suspended pipeline length of 300 m, internal pressure of 12 MPa, non-penetrating defect depth of 13 mm, type-B sleeve with a length of 1 m, and located at the middle of the suspended pipeline, the mechanical behavior was calculated. As Figure 8 depicts, high Mises stress (M_S) zones for penetrating and non-penetrating pipelines were located at junctional regions of the suspended segment of the pipeline. The peak M_S value is measured to be 613 Mpa, exceeding the yield strength repaired type-B sleeve. However, the M_S on the type-B sleeve with a penetrating defect is a notable difference from that with a non-penetrating defect.

As Figure 9a shows, high stress concentration was observed at the bottom of the fillet weld for both these types of defective pipelines, with a slightly higher value for the pipeline with penetrating defects (453 Mpa) compared to the one with non-penetrating defects (415 Mpa). The Mises stress distribution on the type-B sleeve was further compared, and a similar trend was observed; as shown in Figure 9b, stress on the sleeve with penetrating defects was larger than that on the one with non-penetrating defects.

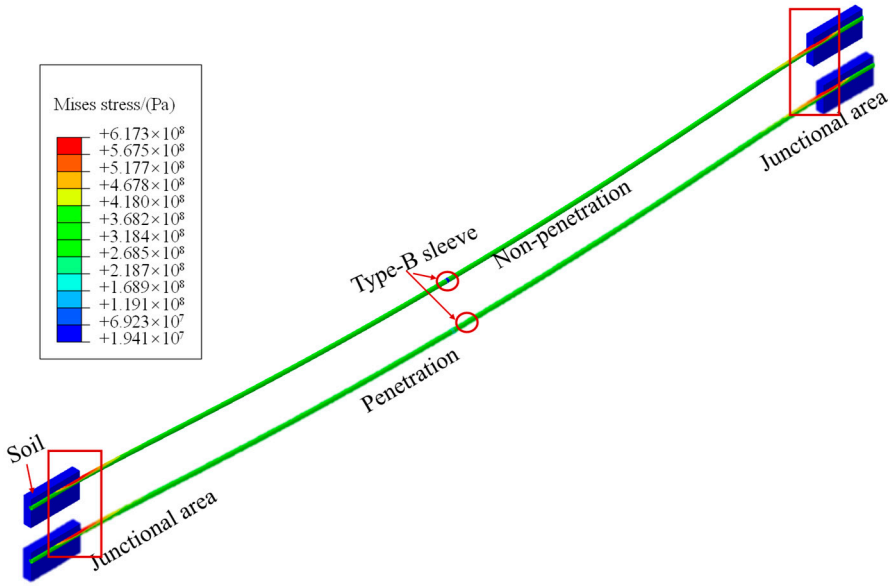


Figure 8. The Mises stress distribution on the pipeline.

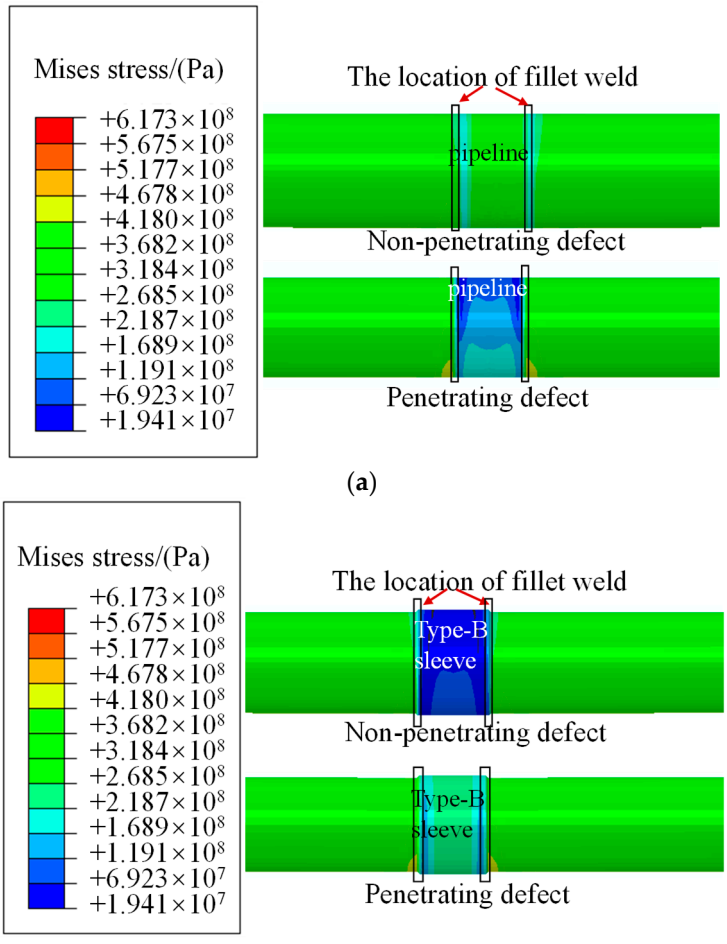
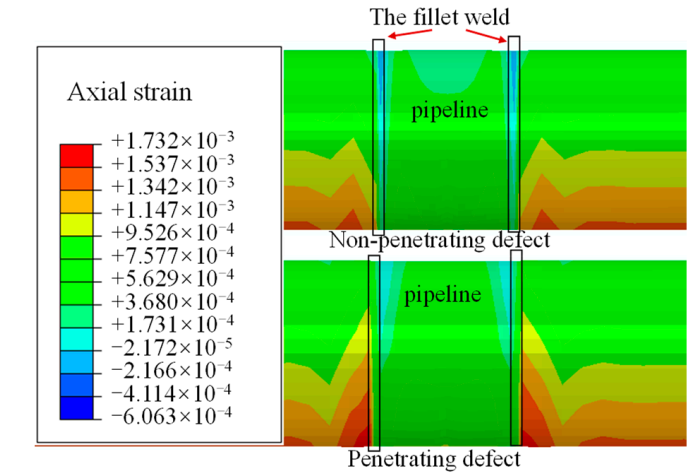


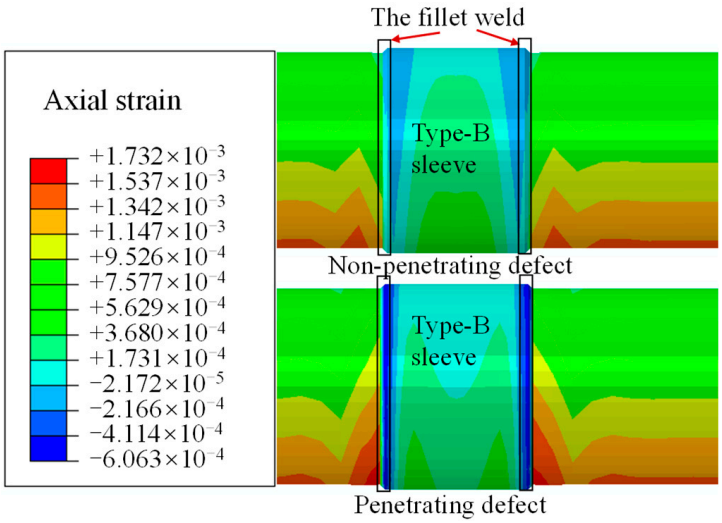
Figure 9. Mises stress distribution. (**a**) The Mises stress distribution on the pipeline. (**b**) The Mises stress distribution on the type-B sleeve.

As seen in Figure 10, the axial strain (ε_a) distribution along the defective pipeline revealed high tensile strain near the bottom of the fillet weld, with the maximum ε_a of the

penetrating defect reaching 1.732×10^{-3}, i.e., higher than that of the non-penetrating defect (1.53×10^{-3}). Figure 10a shows that regardless of whether or not the defect penetrates the pipeline wall, the axial strain value and distribution on the pipeline between the two fillet welds were mostly similar. For the type-B sleeve, Figure 10b demonstrates that although the magnitude of the axial strain varied, the distribution pattern essentially remained consistent. The axial strain changed from tension to compression upon moving from the pipeline to the type-B sleeve. However, for the pipeline with penetrating defects, the compressive strain value at the fillet weld zone exceeded -6×10^{-4}, i.e., significantly higher than that at the fillet weld zone of the pipeline with non-penetrating defects (-2.17×10^{-5}). Comparing the results for the two situations indicates that the failure risk increased for the type-B sleeve with the defect penetrating the pipeline wall. Therefore, we chose the pipeline with penetrating defects for the subsequent simulations. Furthermore, the M_S and ε_a values at the bottom of the type-B sleeve were higher and more complex than those at its top. Therefore, as Figure 11 shows, the axial paths along the bottom of the type-B sleeve and circumferential paths along the fillet weld are chosen to investigate the mechanical behavior of the type-B structure.



(**a**)



(**b**)

Figure 10. The axial strain distribution. (**a**) The axial strain on the pipeline. (**b**) The axial strain on the type-B sleeve.

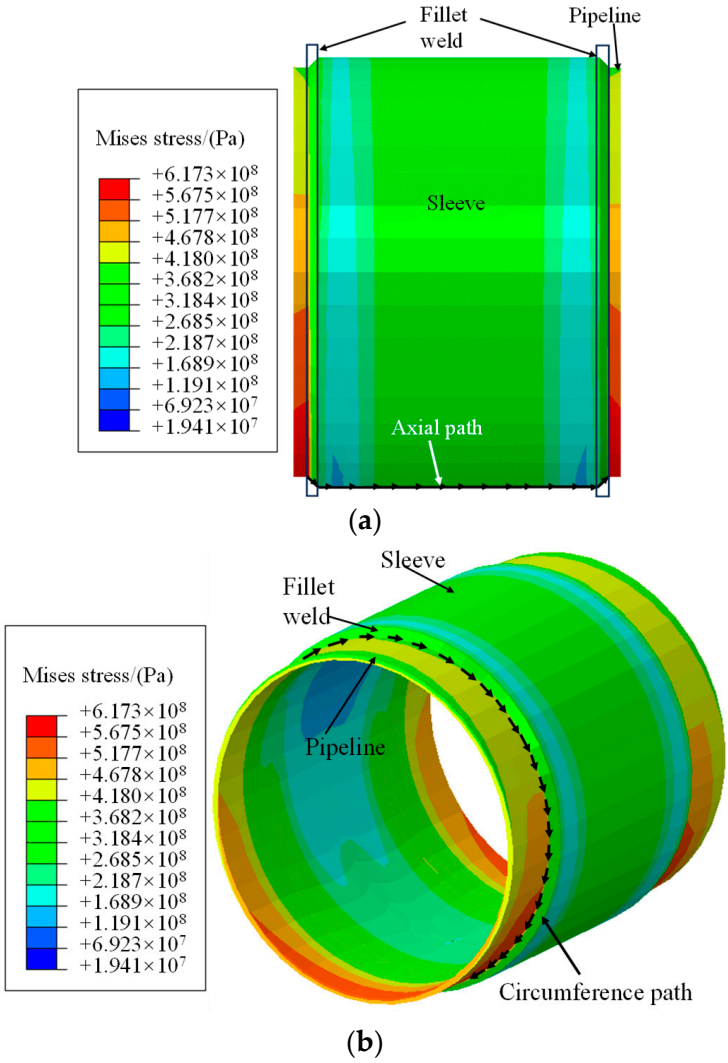


Figure 11. The selected path. (**a**) Axial path. (**b**) Circumferential path.

3.2. Effect of Type-B Sleeve Location

Figure 3 shows that the type-B sleeve location on the suspended pipeline is defined as the distance between the symmetric plane of the type-B sleeve and soil, which is represented by *s*. The effect of the type-B sleeve location on the M_S and ε_a along the axial path is shown in Figure 12. The Mises stress is found to be the highest at the fillet weld. As shown in Figure 12a, along the axial path, the M_S on the fillet weld increases from 339 MPa at s = 0 man to 453 Mpa at *s* = 150 m. For the type-B sleeve, at *s* = 0 m, the M_S is 395.8 Mpa, i.e., higher than any other sleeve location, while the M_S remains nearly constant at the central region of the sleeve for all locations. The load acting on the sleeve is transmitted through fillet welds during pipeline suspension. Due to the length of the sleeve being much shorter than the suspended pipeline length, the difference in load values between the two ends of the type-B sleeve is not significant. Therefore, little distinction is observed in the axial strain and Mises stress at the central regions of the type-B sleeve.

Figure 12b shows the axial stain along the axial path and reveals that the two fillet welds experienced asymmetric stresses when the type-B sleeve was not placed at the center of the suspended pipeline, resulting in unequal loads on both fillet weld locations. At *s* = 0 m, the ε_a along the axial path is compressive. Except for s = 0, the peak axial compressive strain (-0.529×10^{-3}) at both sleeve ends for all sleeve locations remains quite similar within an error of 0.04×10^{-3}. The strain alternated between tension and

compression at both sleeve ends. For s = 150 m, the highest axial tensile strain increases to 1.662×10^{-3}.

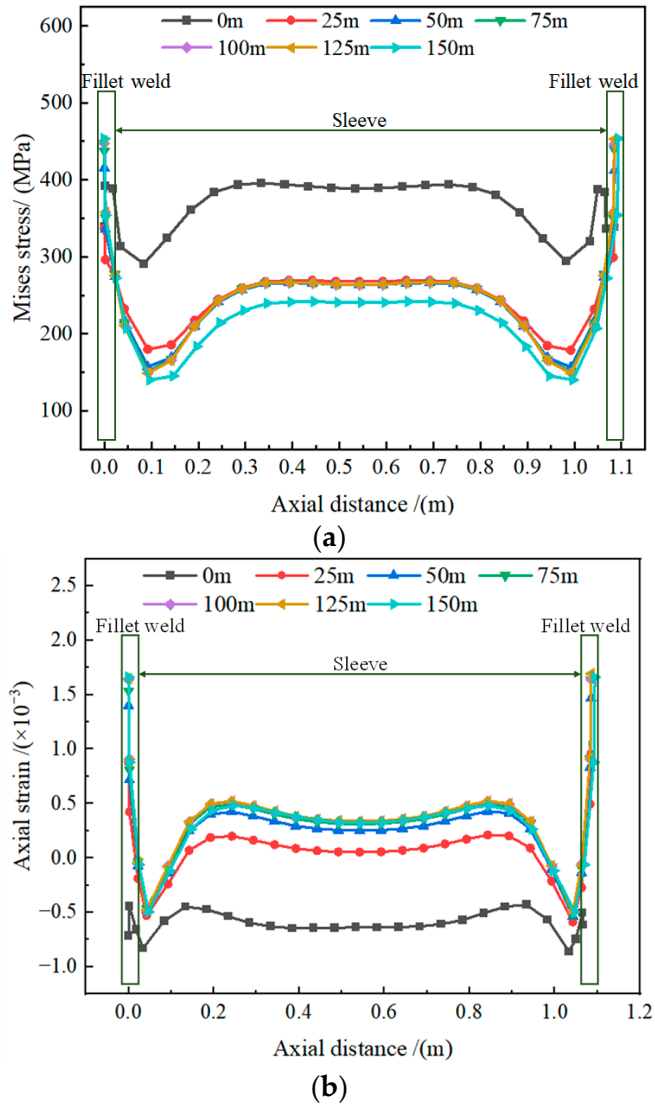


Figure 12. The Mises stress distribution along the axial distance. (**a**) Mises stress along the axial reference path. (**b**) Axial strain along the axial reference path.

The Mises stress and axial strain at the fillet weld along the circumferential paths are shown in Figure 13. Figure 13a shows that when the distance s increases, the stress at the top (bottom) of the fillet weld tends to decrease (increase). At s = 0 m, the peak M_S at the top of the fillet weld is 602 MPa, exceeding the yield strength stress of the API 5L X80 pipeline steel. Along the circumferential path, as shown in Figure 13b, the peak axial tensile strain is observed to be 5.5×10^{-3} for s = 0 m, which decreases to 2.2×10^{-3} at s = 150 m. Therefore, when the sleeve position settles closer to the edge of the suspended portion of the pipeline, the failure risk of the sleeve construction increases.

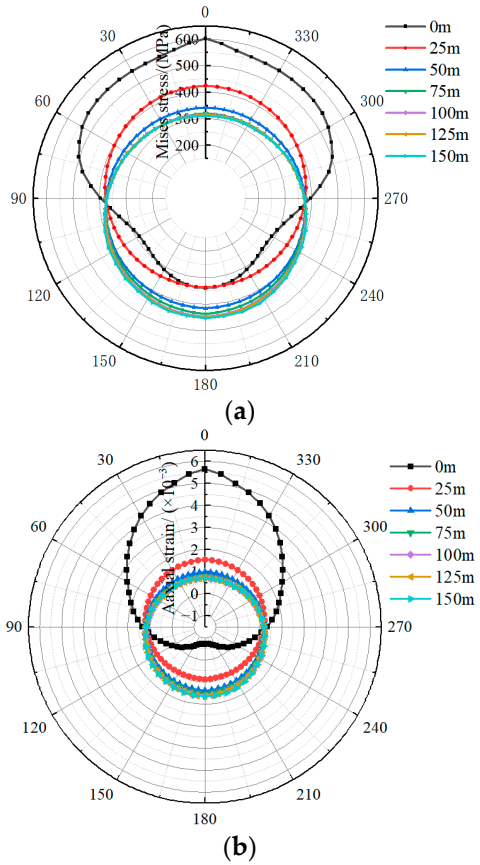


Figure 13. The Mises stress and axial strain along the circumferential path. (**a**) The Mises stress distribution. (**b**) The axial strain distribution.

3.3. Effect of the Sleeve Length

Figure 14 illustrates the influence of the length of the type-B sleeve on the M_S and ε_a along the axial path. It can be seen from Figure 14a that the peak Mises stress is at the fillet weld; the M_S value in the middle region of the sleeve is not affected by the length of the sleeve. When the length of the type-B sleeve increases from 1 to 3 m, the Mises stress at the (i) fillet weld increases from 453 MPa to 468 Mpa, and (ii) the adjacent to the fillet weld position grows from 130 Mpa to 175 Mpa. This is due to the axial force and shear force on the cross-section experiencing negligible change with the sleeve length increasing from 1.0 to 3.0 m. Moreover, the large diameter and wall thickness weaken the load on the fillet weld and sleeve.

Figure 14b shows that except sleeve length of 1.5 m, the maximum axial tensile strain and compressive strain have a positive and negative correlation with the sleeve length, respectively. At the sleeve length of 1 m, the peak axial tensile strain and compressive strain are 0.7×10^{-3} and -0.56×10^{-3}, respectively. When the length of the type-B sleeve increases to 3 m, the axial tensile strain increases to 1.72×10^{-3} and compressive strain reduces to -0.25×10^{-3}. In particular, at a sleeve length of 1.5 m, the peak tensile and compressive ε_a are 1.57×10^{-3} and -0.15×10^{-3}, respectively.

Along the circumferential path, near the bottom of the fillet weld, the Mises stress increased from 453 to 468 MPa as the sleeve length increased from 1.0 to 3.0 m, which is shown in Figure 15a. However, the stress values near the top of the fillet weld are less affected by the sleeve length; the M_S increased from 311 Mpa for a sleeve length of 1.0 m to 314 Mpa for a sleeve length of 3.0 m. Figure 15b demonstrates that the axial strain at the top of the fillet weld is 0.69×10^{-3} at the sleeve length of 1 m, i.e., only marginally greater than the axial strain at other sleeve lengths. At the bottom of the fillet weld, the ε_a increases from 1.66×10^{-3} to 1.72×10^{-3} as the length of the type-B sleeve increases from 1 to 3 m.

The results indicate that stress and strain can be reduced to a certain extent by selecting the appropriate sleeve length, thereby increasing the bearing capacity of the type-B sleeve.

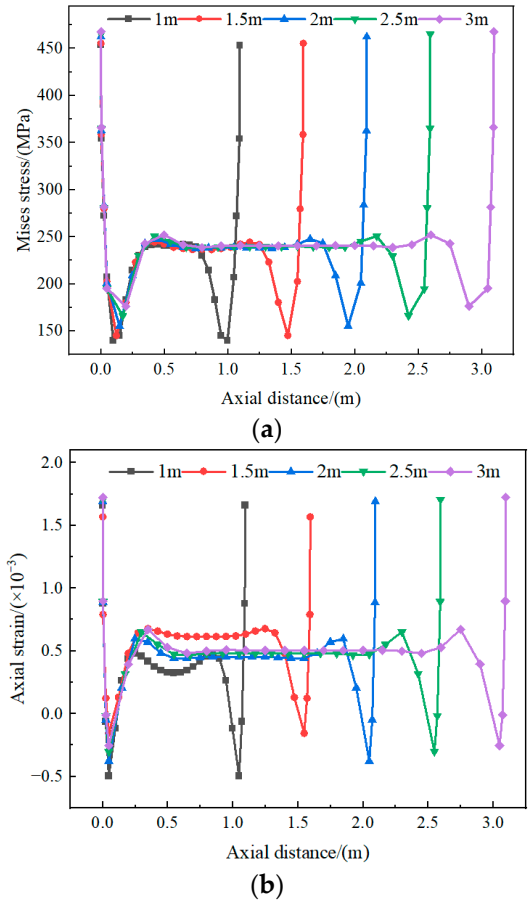


Figure 14. The Mises stress and axial strain distributed along the axial path. (**a**) The Mises stress along the axial path. (**b**) The axial strain along the axial path.

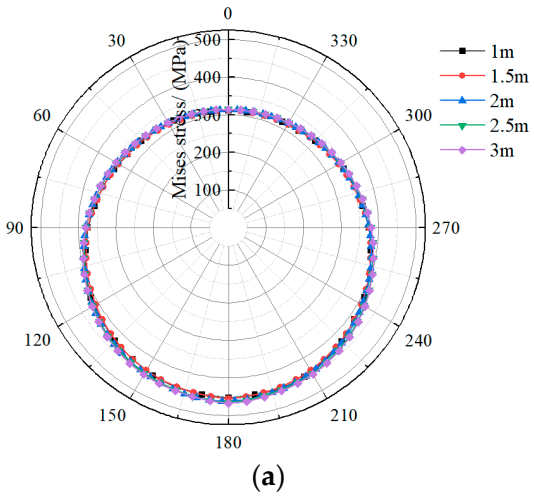
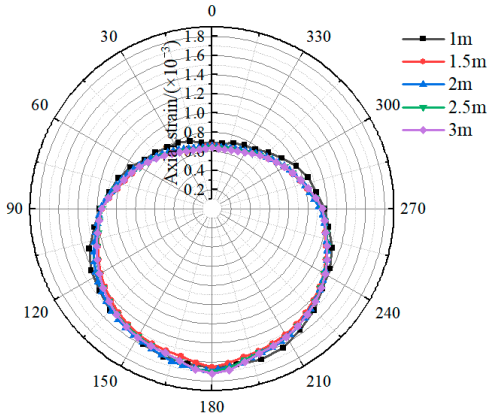


Figure 15. *Cont*.



(**b**)

Figure 15. The Mises stress and axial strain along the circumferential path. (**a**) The Mises stress distribution along the circumferential path. (**b**) The axial strain distribution along the circumferential path.

3.4. Effect of the Defect Location

Figure 16 illustrates the location of the defect on the pipeline, which is represented by θ. Figure 17 shows the effect of the defect's position on the mechanical behavior of the type-B sleeve along the axial path. As illustrated in Figure 17a, the peak Mises stress is observed at the fillet weld of the type-B sleeve. When the defect position varies from 0° to 180°, the M_S at every position of the axial path remains virtually constant. The peak M_S at the fillet weld is 447 MPa, while the M_S at the middle region of the sleeve remains 241 Mpa.

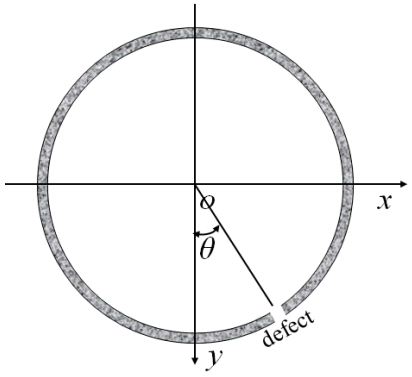
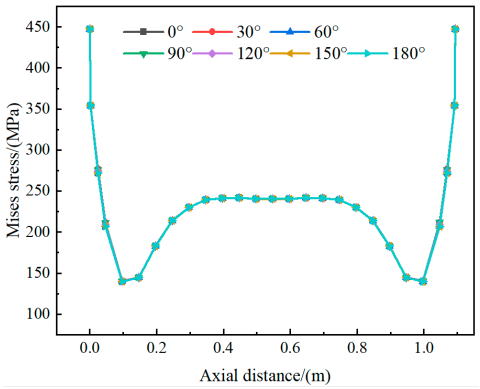
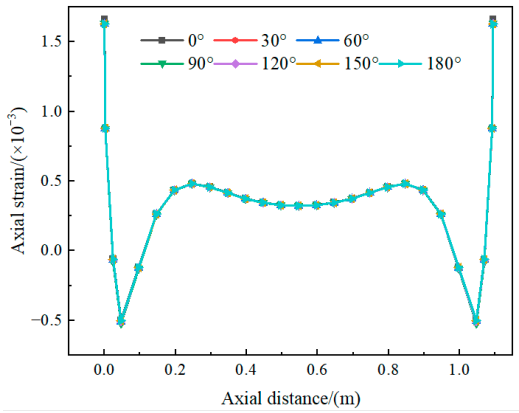


Figure 16. The defect location (θ) on the pipeline.



(**a**)

Figure 17. *Cont.*

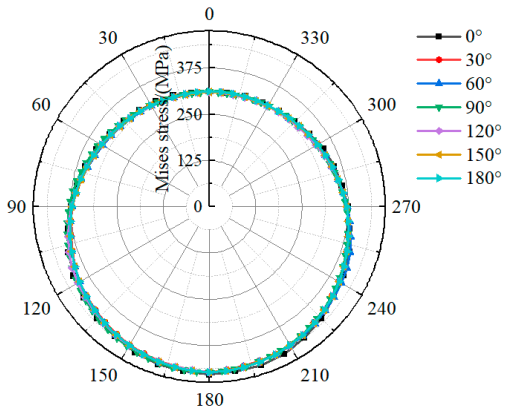


(**b**)

Figure 17. The Mises stress and axial strain distribution along the axial path. (**a**) The Mises stress distribution along the axial path. (**b**)The axial strain distribution along the axial path.

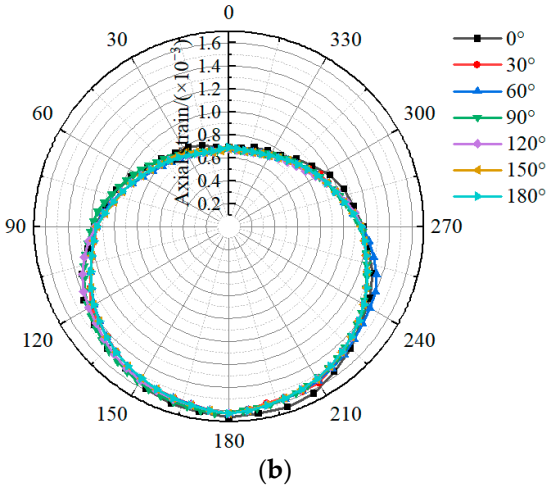
Along the axial reference path, for $\theta = 0°$, the ε_a at the fillet weld was 1.66×10^{-3}, which is shown in Figure 17b. However, an axial strain difference of only 0.03×10^{-3} is observed at the fillet weld between the defect at $\theta = 0°$and other positions, i.e., except for at $\theta = 0°$, the ε_a values appear to be the same at every point along the axial path. Therefore, the defect location on the pipeline is determined to have little relation with the load acting on the type-B sleeve.

The influence of defect location on the Mises stress and axial strain of the fillet weld along the circumferential path is shown in Figure 18. It can be found in Figure 18a that only minor changes are observed in M_S at each point on the circumferential path as the defect position shifts from 0° to 180°. For $\theta = 0°$, the M_S at the top and bottom of the fillet weld are 311 MPa and 453 Mpa, respectively. The relationship between the axial strain of the fillet weld and the defect location is shown in Figure 18b. It can be seen that ε_a at 90° and 270° on the circumferential path slightly fluctuates with the change in the defect position. For $\theta = 0°$ and 180°, the ε_a is 1.45×10^{-3} and 1.40×10^{-3}, respectively. In general, the load on the sleeve remains unchanged when the defect location changes. Therefore, the stress and strain distribution indicate that the location of the defect on the pipeline has little effect on the mechanical behavior of the type-B sleeve.



(**a**)

Figure 18. *Cont.*

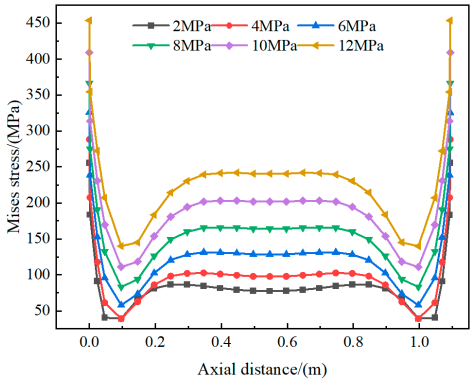


(**b**)

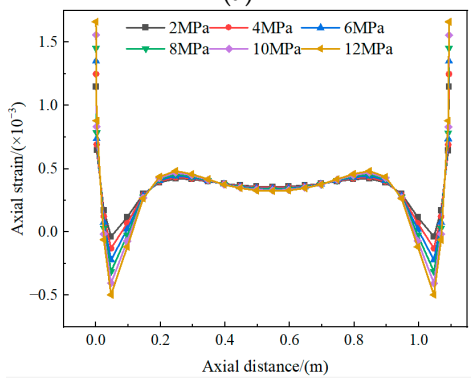
Figure 18. The Mises stress and strain of fillet weld along the circumferential path. (**a**) Mises stress distribution. (**b**) Axial strain distribution.

3.5. Effect of the Internal Pressure

Figure 19a illustrates the Mises stress at each point of the axial path with increasing internal pressure. As the internal pressure increases from 2 MPa to 12 Mpa, the M_S (i) at the fillet weld increases from 255 Mpa to 453 Mpa, and (ii) in the middle section of the sleeve increases from 77 Mpa to 241 Mpa.



(**a**)



(**b**)

Figure 19. The effect of internal pressure on Mises stress and axial strain along the axial path. (**a**) Mises stress distribution. (**b**) Axial strain distribution.

Figure 19b shows that the axial strain at the ends of the sleeve increases with the internal pressure growing along the axial path, while that in the middle region of the type-B sleeve remains at 0.35×10^{-3}. At the fillet weld, the peak ε_a of the axial path is 1.15×10^{-3}

for the 2 MPa, which increases to 1.66 × 10^{-3} as the internal pressure reaches 12 Mpa. When the pressure is less than 2 Mpa, the axial strain is tensile along the axial path and gradually transitions from tensile to compressive at both ends of the sleeve as the internal pressure exceeds 2 Mpa.

Figure 20a shows that the Mises stress at every point on the circumferential path increases with growing internal pressure. When the internal pressure increases from 2 Mpa to 12 Mpa, the M_S at (i) the top of the fillet weld increases from 84 Mpa to 311 Mpa, and (ii) the bottom of the fillet weld increases from 255 Mpa to 453 Mpa. Similarly, for 2 Mpa, the ε_a at the top and bottom of the fillet weld are 0.32 × 10^{-3} and 1.15 × 10^{-3}, respectively, which increases 1.15 × 10^{-3} and 1.66 × 10^{-3}, respectively, as the pressure reaches 12 Mpa. Therefore, it is clear that the internal pressure has less impact on the axial strain at the top of the weld than at its bottom.

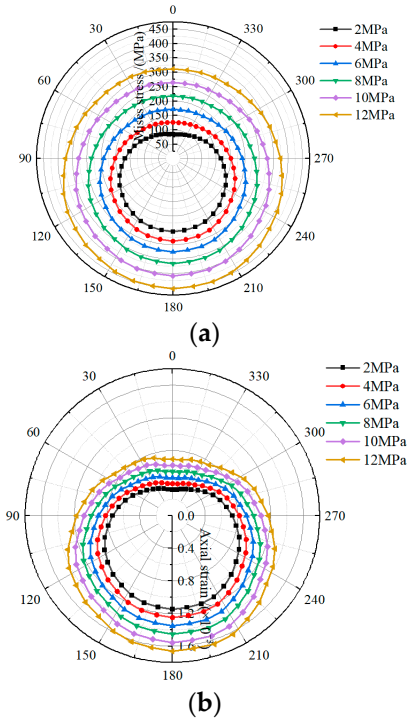


Figure 20. The Mises stress and axial strain along the circumferential path. (**a**) Mises stress distribution. (**b**) Axial strain distribution.

As Equations (11)–(13) show, the internal pressure applied on the pipeline and type-B sleeve is an important factor affecting the stress and strain. Radial stress, axial stress, and the circumferential stress caused by internal pressure can be expressed as:

$$\sigma_r = -p \tag{11}$$

$$\sigma_{ap} = \mu p(d - 2t)/2t \tag{12}$$

$$\sigma_c = \frac{p(d - 2t)}{2t} \tag{13}$$

where the σ_r, σ_{ap}, and σ_c are radial stress, axial stress, and circumferential stress, respectively; t is the pipeline wall thickness; μ is the Poisson's ratio.

3.6. Effect of the Suspended Pipeline Length

Figure 21a shows that the Mises stress at the fillet weld is 386 MPa for a suspended pipeline length of 100 m, which increases to 503 Mpa at a suspended pipeline length of 600 m. It also can be observed that the M_S at every point of the middle region of the type-B sleeve is equal between the suspended pipeline lengths of 200 to 500 m. Furthermore, the

M_S along the axial path also follows a similar trend for the suspended pipeline lengths of 100 and 600 m.

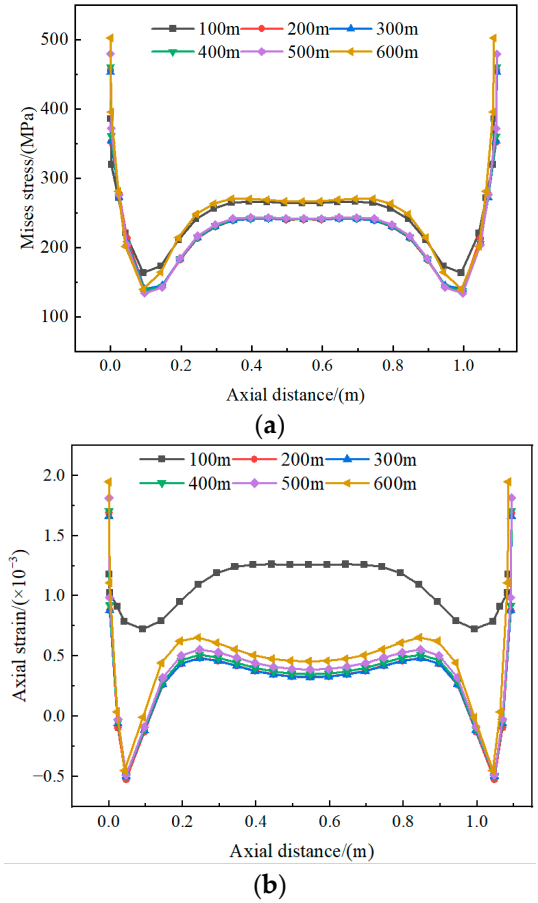


Figure 21. The Mises stress and axial strain distribution along the axial path. (**a**) Mises stress distribution; (**b**) Axial strain distribution.

As depicted in Figure 21b, along the axial path, the peak axial strain is observed at the fillet weld, and its value increases from 1.18×10^{-3} to 1.94×10^{-3} when the suspended pipeline length increases from 100 m to 600 m. When the suspended pipeline length is 100 m, the axial strain along the axial path remains tensile. However, tensile and compressive strains distribute along the axial path when the length of the suspended pipeline exceeds 200 m. The axial compressive strain value decreases only by 0.07×10^{-3} as the suspended pipeline length increases from 200 to 600 m.

Figure 22 illustrates the relationship between suspended pipeline length and Mises stress and axial strain along the circumferential path. It is found that as the suspended pipeline length increases from 100 m to 600 m, the M_S at the top and bottom of the fillet weld increases from 288 MPa to 416 Mpa and 386 Mpa to 502 Mpa, respectively (Figure 22a). Thus, the influence of suspended pipeline length on the Mises stress at the top of the fillet weld is higher than that at its bottom.

In Figure 22b, the ε_a distribution along the fillet weld reveals that the longer the suspended pipeline length, the greater the ε_a at each point of the fillet weld. When the suspended pipeline length is 100 m, the axial strain at the top point of the circumferential path is compressive, with a value of -0.39×10^{-3}. The axial strain at the bottom of the fillet weld increases from 1.27×10^{-3} to 1.95×10^{-3} as the suspended pipeline length increases from 100 m to 600 m.

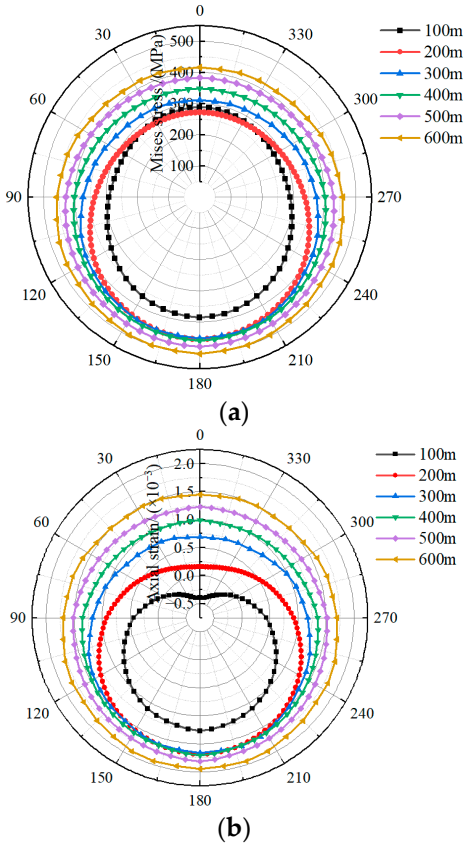


Figure 22. The Mises stress and axial strain distribution of fillet weld along the circumferential path. (**a**) Mises stress distribution; (**b**) Axial strain distribution.

The results show that the length of the suspended pipeline has an important effect on the mechanical behavior of the type-B sleeve, but an increase in suspended pipeline length may not always be harmful to the middle region of the sleeve.

4. Conclusions

In this study, a numerical model of a pipeline reinforced with a type-B sleeve was established while considering the effect of the pipeline–soil interaction and penetrating defect, and its mechanical behavior was investigated under suspension. The primary conclusions of our study are detailed as follows.

The strength of the defective pipeline significantly improved after repairing it with a sleeve. The Mises stress (i) around the defect decreased, and (ii) at the fillet weld increased after the type-B sleeve installation.

Due to the effects of the bending moment and shear force generated by suspension, peak Mises stress and axial strain values were observed at the ends of the suspended section of the pipeline, which were unaffected by the position of the type-B sleeve. Therefore, the closer the sleeve position is to the end of the suspended section, the greater the risk of failure.

A comparison of the Mises stress and axial strain distribution in the type-B sleeve structures revealed that the fillet weld is the most prone to failure. Natural gas pressure and suspended pipeline length are the key load factors affecting the mechanical behavior of the welds.

As the length of the sleeve increased from 1 to 3 m, the additional peak Mises stress and tensile axial strain values on the sleeve did not exceed 14 MPa and 0.06×10^{-3}, respectively.

When settlement occurs, the maximum Mises stress and axial strain values were observed at the fillet weld for the type-B sleeve structure; the axial strain alternated between tension and compression. Both Mises stress and axial strain experienced an increase with

the increasing suspended pipeline length, inter-al pressure, and type-B sleeve length, but they were almost independent of the defect location on the pipeline.

The results of this study suggest that reducing natural gas transportation pressure and optimizing sleeve structure parameters can diminish the risk of sleeve failure due to suspension.

Author Contributions: Conceptualization, G.Q.; Methodology, H.T. and Y.D.; Software, H.T., Y.D. and G.Q.; Validation, Z.L. and Z.D.; Formal analysis, Y.D.; Investigation, H.T.; Resources, G.Q. and Z.D.; Data curation, H.T. and G.Q.; Writing—original draft preparation, H.T. and Y.D.; writing—review and editing, H.T. and G.Q.; Visualization, H.T.; Supervision, Y.D.; Project administration, H.T. and Z.D.; Funding acquisition, H.T. All authors have read and agreed to the published version of the manuscript.

Funding: This work is supported by Key Projects of Civil Aviation Flight Academy of China (Grant: J2021-104) and Civil Aviation Administration Education Talent Program (Grant: MHJY2023025). The authors appreciated the support of Key Projects of Sichuan Vocational and Technical College of Architecture (Grant: 2022KJ04).

Data Availability Statement: Data are contained within the article.

Conflicts of Interest: Guangyou Qiu was employed by the Pipe China The remaining authors declare that the research was conducted in the absence of any commercial or financial relationships that could be construed as a potential conflict of interest. The authors declare that they have no known competing financial interests or personal relationships that could have appeared to influence the work reported in this paper.

References

1. Zhang, Y.M.; Yi, D.K.; Xiao, Z.M.; Huang, Z.H. Engineering critical assessment for offshore pipelines with 3-D elliptical embedded cracks. *Eng. Fail. Anal.* **2015**, *51*, 37–54. [CrossRef]
2. Zheng, Q.; Xu, Q.; Shu, Z.; Yang, D.; Chen, W.; Akkurt, N.; Zhang, H.; Lin, L.; Zhang, X.; Ding, Y. A review of advances in mechanical behaviors of the underground energy transmission pipeline network under loads. *Gas Sci. Eng.* **2023**, *117*, 205074. [CrossRef]
3. Zhang, J.; Gu, X.; Zhou, Y.; Wang, Y.; Zhang, H.; Zhang, Y. Mechanical properties of buried gas pipeline under traffic loads. *Processes* **2023**, *11*, 3087. [CrossRef]
4. Lim, K.S.; Azraai, S.N.A.; Yahaya, N.; Md Noor, N.; Zardasti, L.; Kim, J.J. Behaviour of steel pipelines with composite repairs analysed using experimental and numerical approaches. *Thin-Walled Struct.* **2019**, *139*, 321–333. [CrossRef]
5. Kec, J.; Černý, I.; Poloch, A.; Kyselá, B.; Poupa, M. Oil transmission pipelines with corrosion defects reinforced by two types of sleeves: Comparison efficiency of sleeves. *Procedia Struct. Integr.* **2022**, *37*, 598–605. [CrossRef]
6. Alexander, C.; Vyvial, B.; Wilson, F. Pipeline repair of corrosion and dents: A comparison of composite repairs and steel sleeves. In Proceedings of the 2014 10th International Pipeline Conference, Calgary, AB, Canada, 29 September–3 October 2014.
7. Huang, Z.; Tang, H.; Ding, Y.; Wei, Q.; Xia, G. Numerical simulations of temperature for the in-service welding of gas pipeline. *J. Mater. Process. Technol.* **2017**, *248*, 72–78. [CrossRef]
8. Vafaei, M.; Mashhuriazar, A.; Omidvar, H.; Sajuri, Z. In-service welding of X70 steel gas pipeline: Numerical and experimental investigations. *J. Mater. Res. Technol.* **2023**, *26*, 6907–6918. [CrossRef]
9. Arif, A.; Al-Nassar, Y.; Al-Qahtani, H. Optimization of Pipe Repair Sleeve Design. *J. Press. Vessel. Technol.* **2012**, *134*, 051702. [CrossRef]
10. Shuai, Y.; Wang, X.; Wang, J.; Yin, H.; Cheng, Y.F. Modeling of mechanical behavior of corroded X80 steel pipeline reinforced with type-B repair sleeve. *Thin-Walled Struct.* **2021**, *163*, 107708. [CrossRef]
11. Sabapathy, P.N.; Wahab, M.A.; Painter, M.J. The prediction of burn-through during in-service welding of gas pipelines. *Int. J. Press. Vessel. Pip.* **2000**, *77*, 669–677. [CrossRef]
12. Yu, C.; Han, C.; Xie, R.; Wang, L. Mechanical behavior analysis of buried pipeline under stratum settlement caused by underground mining. *Int. J. Press. Vessel. Pip.* **2020**, *188*, 104212. [CrossRef]
13. Liu, M.; Ortega, R. Assessment of impact to buried pipelines due to tunneling-induced settlement. *J. Pipeline. Syst. Eng. Pract.* **2023**, *14*, 04023020. [CrossRef]
14. Ma, C.; Cheng, X.; Xu, T. Research on local buckling failure range of X80 buried steel pipeline under oblique-reverse fault. *Soil Dyn. Earthq. Eng.* **2023**, *164*, 107592. [CrossRef]
15. Zhang, J.; Xie, R. Mechanical Behavior analysis of suspended Pipelines caused by ground subsidence. *J. Pipeline. Syst. Eng. Pract.* **2021**, *12*, 04021030. [CrossRef]
16. Shuai, Y.; Wang, X.; Cheng, Y. Buckling resistance of an X80 steel pipeline at corrosion defect under bending moment. *J. Nat. Gas. Sci. Eng.* **2021**, *93*, 104016. [CrossRef]

17. Cheng, X.; Ma, C.; Huang, R.; Huang, S.; Yang, W. Failure mode analysis of X80 buried steel pipeline under oblique-reverse fault. *Soil Dyn. Earthq. Eng.* **2019**, *125*, 105723. [CrossRef]
18. Shang, B.; Li, C.; Lu, H. Stress analysis of suspended gas pipeline segment. *J. Pipeline Syst. Eng. Pract.* **2017**, *8*, 04017003. [CrossRef]
19. Zhang, B.; Chen, F.; Wang, Q. Analytical model of buried beams on a tensionless foundation subjected to differential settlement. *Appl. Math. Model.* **2020**, *87*, 269–286. [CrossRef]

Disclaimer/Publisher's Note: The statements, opinions and data contained in all publications are solely those of the individual author(s) and contributor(s) and not of MDPI and/or the editor(s). MDPI and/or the editor(s) disclaim responsibility for any injury to people or property resulting from any ideas, methods, instructions or products referred to in the content.